JOURNAL OF GUIDANCE, CONTROL, AND DYNAMICS
Vol. 31, No. 6, November–December 2008

Optimal and Feedback Path Planning for Cooperative Attack

Andrew J. Sinclair*
Auburn University, Auburn, Alabama 36849
Richard J. Prazenica†
Radiance Technologies, Huntsville, Alabama 35805
and
David E. Jeffcoat‡
U. S. Air Force Research Laboratory, Eglin Air Force Base, Florida 32542

DOI: 10.2514/1.35599

This paper considers cooperative path planning for aerial munitions during the attack phase of a mission against ground targets. It is assumed that sensor information from multiple munitions is available to refine an estimate of the target location. Based on models of the munition dynamics and sensor performance, munition trajectories are designed that enhance the ability to cooperatively estimate the target location. The problem is posed as an optimal control problem using a cost function based on the variances in the target-location estimate. These variances are computed by fusing the individual munition measurements in a weighted least-squares estimate. Solutions to the problem are found using a direct-shooting method. These solutions are compared with trajectories developed by an alternative suboptimal feedback-guidance law. This feedback law produces solutions with far less numerical expense and with a performance very close to the best known solutions. The reduction in target-location uncertainty associated with these trajectories could enable the attack of targets with greater precision using smaller, cheaper munitions.

I. Introduction

RESEARCH is in progress on the cooperative control of air armament designed to detect, identify, and attack ground targets. One class of this type of armament is wide-area search munitions, which can be deployed in an area of unknown targets. Current development is focused on possibilities of enhancing munition capabilities through cooperative control. This paper presents a new concept for developing trajectories that enhance munitions' capability to cooperatively estimate target locations. The concept uses a second munition in the local battle area to help improve the target-location estimate during an attack. After the attack is completed, the second munition can continue its own mission. Although many guidance methods do not require full knowledge of the target state, an accurate estimation of the target location can be important for reasons such as impact-angle shaping.

The tasks of intercepting a chosen target and estimating the target's location can represent competing requirements in the path planning of a munition. In a general sense, the problem posed here is to plan a path to a target while simultaneously estimating that target's location. This can be considered a simultaneous-localization-and-planning (SLAP) problem. Whereas SLAP problems can be studied for a single agent, many interesting behaviors emerge when cooperative agents are considered.

Important work exists in the literature on the two related problems of cooperative search [1–3] and the design of optimal trajectories for single observers [4–12]. Much of the work in optimal trajectories has focused on bearings-only measurements of a target, often related to sonar applications. Speyer et al. studied homing-missile trajectories to improve missile–target relative-state estimation in the presence of radar glint [4]. Fawcett investigated the impact of maneuvers on the Cramer–Rao lower bound for the target-state estimate [6]. Frew and Rock investigated a method to minimize a measure of the estimate error covariance [11].

Other works, by Grocholsky [13] and Ousingsawat and Campbell [14], have combined these features in the study of optimal trajectories for cooperative observers. These works have focused on the reconnaissance of a target, relating the performance index to the quality of the target-location estimate at the end of the mission or a time interval. The work presented here differs from those previous works by focusing on cooperative attack rather than cooperative reconnaissance. Distinguishing features of the current work include fixed boundary conditions, a free final time, and a cost function that encourages reduction in uncertainty early in the mission.

Several related topics have also been studied that capture aspects of both cooperative search and trajectory design. Dohner et al. used a Lyapunov approach to drive a vehicle swarm to an uncertain target location while simultaneously maintaining swarm spacing to ensure observability of the target [15]. Passino et al. developed a distributed cooperative search algorithm in which decisions were made to minimize a cost function representing several subgoals, such as covering areas of large uncertainty and minimizing overlap with other agents [16]. It is noteworthy that the problem considered in this paper, trajectory design to enhance target-location estimation, is in some ways the dual of another problem that has received considerable attention, that is, trajectory design to minimize detection by an enemy radar [17–20]. Pachter et al. considered another related problem that used cooperative vehicles to project phantom tracks to an enemy radar [21,22].

This paper extends the field of optimal observer trajectories to the cooperative-attack application. The other main contribution of this paper is the development of a suboptimal feedback-guidance law for cooperative path planning. The motivation for this approach is to capture the properties of the optimal trajectories with a guidance law that can be used in real-time implementation. In the following section, models for the munition motion and sensor performance are presented, and the SLAP trajectory design is posed as an optimal control problem. Next, two different solution methods are presented: direct shooting and suboptimal feedback guidance. Finally, the performance of a target-location estimation algorithm is evaluated

Received 9 November 2007; revision received 16 May 2008; accepted for publication 23 May 2008.

*Assistant Professor, Department of Aerospace Engineering, 211 Davis Hall; sinclair@auburn.edu. Member AIAA.
†Guidance Engineer, 350 Wynn Drive; rprazenica@radiancetech.com. Member AIAA.
‡Senior Research Engineer, Munitions Directorate, 101 West Eglin Boulevard; david.jeffcoat@eglin.af.mil.

along the SLAP trajectories and compared with alternative trajectories.

II. Problem Description

The following developments will describe a problem involving two munitions and one target in a two-dimensional plane. A generalized form of the problem, however, could include larger numbers of targets and munitions in three dimensions. The state of each munition is given by its position in two-dimensional space, $\mathbf{x}_1 = [\,x_1 \quad y_1\,]^\mathsf{T}$ and $\mathbf{x}_2 = [\,x_2 \quad y_2\,]^\mathsf{T}$. A constant-speed kinematic model is used to describe the motion of the munitions. The heading angles of the munitions are ψ_1 and ψ_2, and the speed of each munition is v.

$$\dot{x}_1 = v\cos\psi_1, \qquad \dot{x}_2 = v\cos\psi_2, \qquad \dot{y}_1 = v\sin\psi_1, \qquad \dot{y}_2 = v\sin\psi_2 \tag{1}$$

$$\dot{\mathbf{x}}_i = \mathbf{f}_i(\psi_i), \qquad i \in \{1, 2\} \tag{2}$$

Here, the heading angles are treated as control variables.

Additionally, each munition is considered to carry a sensor that is capable of measuring the target location in the xy plane. Again, the end goal will be to design trajectories that improve the estimation of the target location. Therefore, a model is needed for the sensor measurements and their uncertainties. The target's position is described by $\mathbf{x}_T = [\,x_T \quad y_T\,]^\mathsf{T}$. The measurement of this target location by each munition, $\tilde{\mathbf{z}}_1 = [\,\tilde{x}_{T,1} \quad \tilde{y}_{T,1}\,]^\mathsf{T}$ and $\tilde{\mathbf{z}}_2 = [\,\tilde{x}_{T,2} \quad \tilde{y}_{T,2}\,]^\mathsf{T}$, is modeled as follows:

$$\begin{aligned} \tilde{x}_{T,1} &= x_T + w_{x,1}(0, \sigma_{x,1}), & \tilde{x}_{T,2} &= x_T + w_{x,2}(0, \sigma_{x,2}) \\ \tilde{y}_{T,1} &= y_T + w_{y,1}(0, \sigma_{y,1}), & \tilde{y}_{T,2} &= y_T + w_{y,2}(0, \sigma_{y,2}) \end{aligned} \tag{3}$$

The measurement errors from the first munition are assumed to be independent of the errors from the second munition. The x and y measurement errors from each individual munition, however, are treated as correlated Gaussian random variables with 0 mean and standard deviations of $\sigma_{x,i}$ and $\sigma_{y,i}$, where $i \in \{1, 2\}$. It is these uncertainties that will drive the trajectory design, and they can be selected to model a particular sensor design.

The error in the target-location measurements from an individual munition is treated as following a 0-mean jointly-Gaussian distribution that is uncorrelated in the downrange and cross-range directions, relative to the true target and munition locations. The errors in these directions, $w_{d,i}(0, \sigma_{d,i})$ and $w_{c,i}(0, \sigma_{c,i})$, can therefore be treated as independent Gaussian random variables. The standard deviations in the downrange and cross-range directions are modeled as functions of the range from the munition to the target:

$$\sigma_{d,i} = 0.1 r_i, \qquad \sigma_{c,i} = 0.01 r_i \tag{4}$$

This models a sensor that is more accurate when close to the target and more accurate in the transverse direction than in the radial direction. Although Eq. (4) is a general model, it is motivated by the characteristics of vision sensors. The uncertainty in the measurement of the target location by the ith munition is illustrated in Fig. 1.

From the downrange and cross-range variables, the errors and the covariance matrix in the x and y coordinates can be found:

$$\begin{bmatrix} w_{x,i} \\ w_{y,i} \end{bmatrix} = \begin{bmatrix} \cos\theta_i & \sin\theta_i \\ -\sin\theta_i & \cos\theta_i \end{bmatrix} \begin{bmatrix} w_{d,i} \\ w_{c,i} \end{bmatrix} \tag{5}$$

$$\begin{aligned} \mathbf{P}_1 &= \begin{bmatrix} \sigma_{x,i}^2 & \sigma_{xy,i} \\ \sigma_{xy,i} & \sigma_{y,i}^2 \end{bmatrix} \\ &= \begin{bmatrix} \cos\theta_i & \sin\theta_i \\ -\sin\theta_i & \cos\theta_i \end{bmatrix} \begin{bmatrix} \sigma_{d,i}^2 & 0 \\ 0 & \sigma_{c,i}^2 \end{bmatrix} \begin{bmatrix} \cos\theta_i & -\sin\theta_i \\ \sin\theta_i & \cos\theta_i \end{bmatrix} \end{aligned} \tag{6}$$

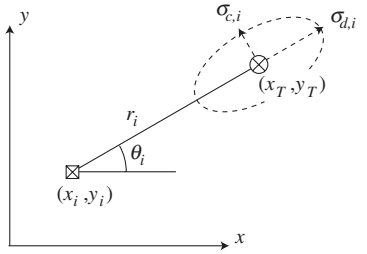

Fig. 1 Measurement of the target by the ith munition and the associated error probability ellipse.

Here, θ_i is the bearing angle of the target relative to the ith munition. The range and bearing angle for each target–munition pair are computed as follows:

$$r_i = \sqrt{(x_T - x_i)^2 + (y_T - y_i)^2} \tag{7}$$

$$\theta_i = \tan^{-1}((y_T - y_i)/(x_T - x_i)) \tag{8}$$

The significance of Eq. (6) is that it models the quality of the measurements from the ith munition based on its position relative to the target.

The measurements provided by both munitions can be fused into a single instantaneous estimate of the target location. This is done using a weighted least-squares estimator (WLSE) [23,24]. The measurements of the target location from each munition are grouped into a measurement vector: $\tilde{\mathbf{z}} = [\,\tilde{x}_{T,1} \quad \tilde{y}_{T,1} \quad \tilde{x}_{T,2} \quad \tilde{y}_{T,2}\,]^\mathsf{T}$. This produces a linear measurement model in terms of the target location:

$$\mathbf{z} = \mathbf{H}\mathbf{x}_T + \mathbf{w} \tag{9}$$

$$\mathbf{H} = \begin{bmatrix} 1 & 0 & 1 & 0 \\ 0 & 1 & 0 & 1 \end{bmatrix}^\mathsf{T}, \qquad \mathbf{W} = [\,w_{x,1} \quad w_{y,1} \quad w_{x,2} \quad w_{y,2}\,]^\mathsf{T} \tag{10}$$

Here, $\mathbf{w}$ is the vector of measurement errors. The covariance of this error vector is given by arranging the covariances from each munition:

$$\mathbf{R} = \begin{bmatrix} \mathbf{P}_1 & \mathbf{0} \\ \mathbf{0} & \mathbf{P}_2 \end{bmatrix} \tag{11}$$

The instantaneous WLSE of the ith target location and the associated covariance are given as follows:

$$\hat{\mathbf{x}}_T = (\mathbf{H}^\mathsf{T}\mathbf{R}^{-1}\mathbf{H})^{-1}\mathbf{H}^\mathsf{T}\mathbf{R}^{-1}\tilde{\mathbf{z}} \tag{12}$$

$$\mathbf{P} = (\mathbf{H}^\mathsf{T}\mathbf{R}^{-1}\mathbf{H})^{-1} \tag{13}$$

Considering the first of Eqs. (10), the WLSE reduces to the following:

$$\hat{\mathbf{x}}_T = \begin{bmatrix} \hat{x}_T \\ \hat{y}_T \end{bmatrix} = (\mathbf{P}_1^{-1} + \mathbf{P}_2^{-1})^{-1}(\mathbf{P}_1^{-1}\tilde{\mathbf{z}}_1 + \mathbf{P}_2^{-1}\tilde{\mathbf{z}}_2) \tag{14}$$

More important for the current purposes, the covariance of this combined estimate is related to the individual covariances of the measurements from each munition:

$$\mathbf{P} = \begin{bmatrix} \sigma_x^2 & \sigma_{xy} \\ \sigma_{xy} & \sigma_y^2 \end{bmatrix} = (\mathbf{P}_1^{-1} + \mathbf{P}_2^{-1})^{-1} \tag{15}$$

The covariance $\mathbf{P}$ now models the quality of the combined target-location estimate based on the positioning of the two munitions relative to the target. For cases with more than two munitions, similar expressions can be developed combining the measurements of each of the munitions. Additionally, for cases with multiple targets,

corresponding expressions can be used for the covariance of each target-location estimate.

The task of designing trajectories for the munitions to enhance the estimation performance can now be posed as the following optimal control problem. Consider the state vector $\mathbf{x} = [\,x_1 \quad y_1 \quad x_2 \quad y_2\,]^{\mathrm{T}}$. The heading angles of the munitions can be organized into a control vector: $\mathbf{u} = [\,\psi_1 \quad \psi_2\,]^{\mathrm{T}}$. The state vector evolves according to the state equation found by grouping Eq. (2): $\dot{\mathbf{x}} = \mathbf{f}(\mathbf{u}) = [\mathbf{f}_1^{\mathrm{T}}\mathbf{f}_2^{\mathrm{T}}]^{\mathrm{T}}$. For boundary conditions, the initial positions of the munitions will be considered a given, and the final position of munition 1 is required to be the target location:

$$x_1(t_F) = x_T, \qquad y_1(t_F) = y_T \tag{16}$$

The final position of munition 2 is free.

The goal will be to find the trajectories that minimize the following cost function, which is based on the WLSE covariance:

$$J = \int_0^{t_F} (\sigma_x^2 + \sigma_y^2)\,\mathrm{d}t \tag{17}$$

The variances of each target location are functions of the states describing the munition configuration. Clearly, this cost function emphasizes the uncertainty over the entire trajectory. Previous works have used performance indices related to the uncertainty at the end of the trajectory or a specified interval [13,14]. Compared with those alternative indices, the cost function used here encourages reduction in uncertainty earlier in the trajectory. It is also noted that other cost functions could be based on the determinant or other metrics of the covariance matrix.

The above conditions have not accounted for limitations in the field of view of the vehicle sensors. This assumes either a sensor that has an unlimited field of view or is gimbal mounted to view a target regardless of the vehicle orientation and heading. A sensor that is fixed mounted on the vehicle, though, may only offer a limited field of view relative to the vehicle heading. In this case, a hard constraint can be enforced on the trajectory of the ith munition to keep the target in view. The field-of-view angle is labeled 2ϕ and is illustrated in Fig. 2.

Two inequality constraint functions can be enforced to keep the target in the field of view of the ith munition. For example, the following constraints keep the target in the field of view of munition 1:

$$c_1 = \psi_1 - \theta_1 - \phi \le 0, \qquad c_2 = -\psi_1 + \theta_1 - \phi \le 0 \tag{18}$$

Note that the bearing angles are functions of the states and the heading angles are the controls.

Based on this description, the optimal control problem is posed to solve for $\psi_1(t)$, $\psi_2(t)$, and t_F to minimize Eq. (17) subject to Eqs. (2), (16), and (18) (unless neglected) and given initial conditions. This problem is nonconvex. Equations (16) (integrations of the nonlinear state equations) are nonlinear functions of $\psi_1(t)$. Additionally, the numerical integration of Eq. (17) for constant heading angles and several candidate values of t_F shows that the cost function is nonconvex with respect to the final time, even though these candidate trajectories do not necessarily satisfy the boundary conditions [25]. It is noteworthy that these features associated with the attack problem, free final time and fixed boundary conditions, are contributing factors to the nonconvexity of the problem.

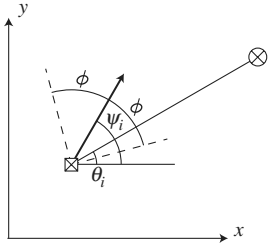

Fig. 2 Heading angle, field-of-view half-angle, and bearing angle of the *i*th munition relative to the target.

For cases with more than two munitions or more than one target, the terminal conditions could be specified by prechosen target–munition attack pairings. The final states for any munitions not assigned a target would be free. For multiple targets, the cost function could be augmented by summing the additional variances from their target-location estimates. For complex scenarios with many targets and munitions, difficulty may arise in the application of the field-of-view constraints. It may be desirable to let targets pass in and out of the field of view of some munitions.

For any scenario, the solution of the problem produces munition trajectories designed to reduce the uncertainty in the target-location estimates. Note that, in a real implementation, the use of the true target positions as boundary conditions would not be possible. These must be estimated, which is the motivation behind the problem in the first place. Here, though, the true locations are used to illustrate the concept and potential benefit of these trajectories.

In the following sections, two different solution methods are presented along with several illustrative examples. In each example, munition 1 is assigned to attack the target and munition 2 is free to assist in the estimation of the target location. A munition speed of $v = 300$ ft/s and a half field-of-view angle of $\phi = 45$ deg are used.

III. Solution by Direct Shooting

In a previous work, the solution to the aforementioned optimal control problem by the indirect method was considered [26]. That method introduced the costates for the problem and derived the associated costate equations from the necessary conditions for an optimal solution. The initial values of the costates were then numerically found using the fsolve package in MATLAB®. In this section, the solution by a direct-shooting method will be described. The problem is converted to a discrete optimization problem by assuming the controls are piecewise constant. The total mission time, t_F, is divided into ten equal increments. This defines ten switching times, including the initial time, at which the munition heading angles are adjusted: $t_i = (i-1)t_F/10$. The heading angles of the munitions are held constant over each increment. The resulting optimization problem, therefore, has a dimension of 21: ten heading angles for each munition and the final time.

Given a candidate solution, the state equations can be solved analytically (due to the choice of piecewise constant controls) and the boundary conditions can be evaluated. Additionally, the cost function can be evaluated with arbitrary accuracy through numerical integration. For the version of the problem applying field-of-view constraints, the original continuous constraints were discretized by applying them only at the beginning of each time increment:

$$\begin{aligned} c_i &= \psi_1(t_i) - \theta_1(t_i) - \phi \le 0,\\ c_{i+10} &= -\psi_1(t_i) + \theta_1(t_i) - \phi \le 0,\\ c_{i+20} &= \psi_2(t_i) - \theta_2(t_i) - \phi \le 0,\\ c_{i+30} &= -\psi_2(t_i) + \theta_2(t_i) - \phi \le 0 \quad \text{for } i = 1,\ldots,10 \end{aligned} \tag{19}$$

The constrained optimization problem was solved using a sequential quadratic programming approach with the fmincon package in MATLAB®. Figure 3a shows the resulting trajectories for initial conditions of $x_1(0) = 0$ ft, $y_1(0) = -2000$ ft, $x_2(0) = 100$ ft, and $y_2(0) = -2000$ ft. The target is located at $x_T = y_T = 0$ ft. Neglecting any field-of-view constraints, this is referred to here as problem 1. The marks along the trajectories in the figure indicate the 10 switching times t_i. The converged solution has a cost of $J = 1.597 \times 10^4$ s · ft^2, as shown in Table 1, and a final time of $t_F = 8.194$ s. These trajectories are very similar to the solution obtained for this problem by the indirect method in [25], and the cost is within 0.27% of that solution. The cost associated with the indirect solution is also shown in Table 1 for comparison.

Munition 1 intercepts the target at t_F as required by the boundary conditions, but munition 2 also approaches the target very closely.

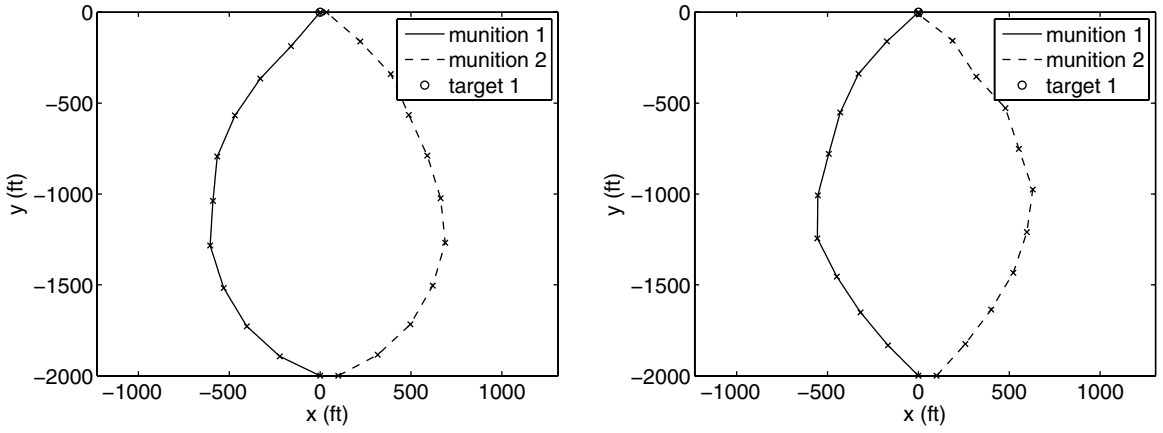

Fig. 3 Direct-shooting trajectories: a) problem 1, and b) problem 2.

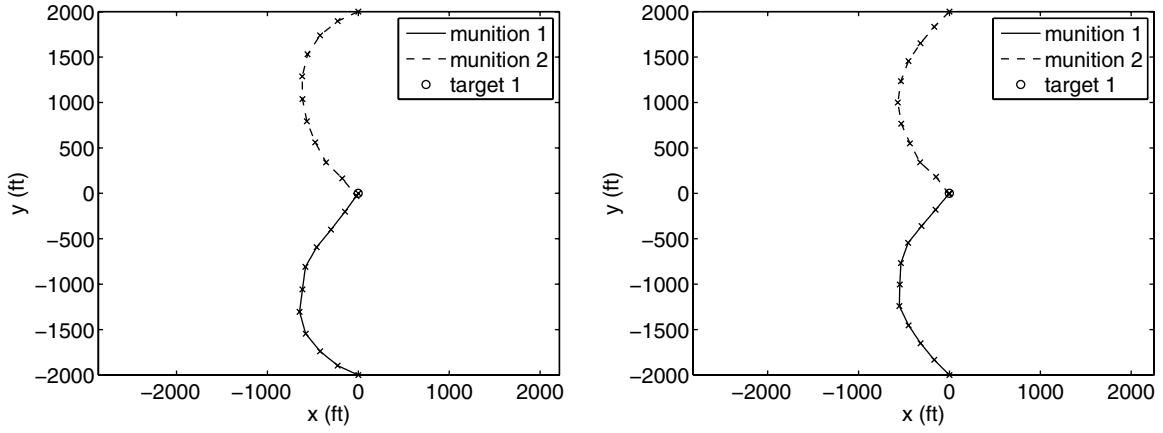

Fig. 4 Direct-shooting trajectories: a) problem 3, and b) problem 4.

Intuitively, this is because the measurement errors from either munition are reduced as the munition closes the range with the target. Instead of traveling directly to the target, however, both munitions sweep out in the $\pm x$ directions near the initial time. This gives the munitions differing perspectives on the target, allowing them to compensate for the relatively large downrange errors in each other's measurements.

In the trajectories for problem 1, both munitions sweep out aggressively such that the target would be out of their fields of view during the initial stages of the trajectories. To correct for this, problem 2 is posed to enforce that both munitions keep the target within view. Problem 2 is identical to problem 1 in all other aspects. The converged solution for this problem results in $J = 1.675 \times 10^4$ s $\cdot$ ft^2 and $t_F = 7.874$ s, and the corresponding trajectories are shown in Fig. 3b. The trajectories found here are qualitatively different than the indirect solution found for this problem in [25]. The current trajectories are more symmetric than the solution in [25]. Additionally, the cost found here is almost 1.4% lower than that solution, indicating that the indirect solution was only a local optimum. It is further noted that the direct method converges to a solution similar to the indirect solution for initial guesses in the neighborhood of that solution.

Next, a different initial condition can be considered with munition 2 moved to an initial position of $x_2(0) = 0$ ft and $y_2(0) = 2000$ ft. Instead of starting near munition 1, munition 2 now starts on the opposite side of the target relative to munition 1. The resulting trajectories are shown in Fig. 4a as problem 3. The cost for these trajectories is $J = 1.897 \times 10^4$ s $\cdot$ ft^2 and the final time is $t_F = 8.323$ s. The trajectories for the two munitions are nearly symmetric about the x axis. Similar to problem 1, the munitions sweep to the side to obtain differing viewpoints before closing in on the target. The cost found here is within 0.24% of the solution found by the indirect method [26].

The solution for these initial conditions when applying the field-of-view constraint is shown as problem 4 in Fig. 4b. The cost associated with this solution is $J = 1.993 \times 10^4$ s $\cdot$ ft^2 and the final time is $t_F = 7.884$ s. Again, these trajectories are qualitatively different than the solutions found in [25], as they are more symmetric about the x axis. Additionally, the cost is 1.4% lower than the solution found by the indirect method, indicating that solution was only a local optimum.

IV. Suboptimal Feedback Solution

The example optimal solutions in Sec. III illuminated two behaviors. These optimal trajectories attempted to close the distance from the munitions to the target and maneuvered the munitions toward orthogonal perspectives of the target. These behaviors are

Table 1 Costs in s $\cdot$ ft^2 for sample problems

Method	Problem 1	Problem 2	Problem 3	Problem 4
Indirect	1.593×10^4	1.698×10^4	1.893×10^4	2.022×10^4
Direct shooting	1.597×10^4	1.675×10^4	1.897×10^4	1.993×10^4
Feedback guidance	1.594×10^4	1.693×10^4	1.894×10^4	2.017×10^4

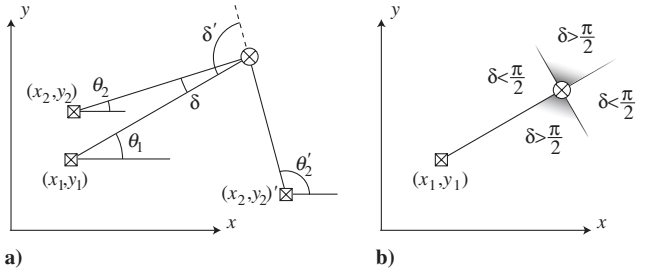

Fig. 5 Relative angle between munitions' lines of sight: a) for two possible locations of munition 2, and b) for various locations of munition 2.

intuitively consistent with the sensor model and cost function used in the problem statement. The identification of these trends, however, motivates the development in this section of a feedback-guidance law that reproduces these behaviors.

The identified behaviors can be expressed in the following suboptimal feedback-guidance laws.

$$\psi_1 = \theta_1 + k_1(\delta)\sin(\delta - \pi/2)$$
$$\psi_2 = \theta_2 - k_2(\delta)\sin(\delta - \pi/2)$$
$$\text{where } \delta = \theta_1 - \theta_2 \pmod{\pi} \tag{20}$$

The angle δ is the relative angle between the munitions' lines of sight and is illustrated in Fig. 5. In the guidance law for each munition, the two terms correlate to the two identified behaviors: the θ_i term guides the munition toward the target, closing the range, and the term proportional to $\sin(\delta - \pi/2)$ maneuvers the munition to a perspective orthogonal to the other munition. Setting $k_1 \neq k_2$ allows one munition to be more responsible for the perspective maneuvering; however, the examples in this work will consider $k_1 = k_2 = k(\delta) \geq 0$. Establishing the guidance law in Eq. (20) reduces the problem to choosing the relative importance of the two behaviors, that is, selecting the gain $k(\delta)$. This gain is written in general as a function of δ to allow the weighting to vary with the relative angle.

Before illustrating the use of Eq. (20), it will be demonstrated that the trajectories generated by the feedback guidance are guaranteed to intercept the target. The desired condition for munition 1 to strike the target can be expressed as $(x_1 - x_T) = (y_1 - y_T) = 0$. It will be convenient, however, to describe the evolution of the system in terms of polar coordinates:

$$r_i = \sqrt{(x_i - x_T)^2 + (y_i - y_T)^2} \qquad x_i - x_T = -r_i \cos\theta_i$$
$$\theta_i = \tan^{-1}\left(\frac{-y_i + y_T}{-x_i + x_T}\right) \quad \leftrightarrow \quad y_i - y_T = -r_i \sin\theta_i \tag{21}$$

In these coordinates, the behavior of r_1 will be investigated. The range rate is taken considering the equations of motion in Eq. (2):

$$\dot{r}_1 = (1/r_1)[(x_1 - x_T)\dot{x}_1 + (y_1 - y_T)\dot{y}_1] = -v\cos(\psi_1 - \theta_1) \tag{22}$$

Next, the guidance law in the first of Eqs. (20) is substituted:

$$\dot{r}_1 = -v\cos(k(\delta)\sin(\delta - \pi/2)) \tag{23}$$

Because $-1 \leq \sin(\delta - \pi/2) \leq 1$, $\dot{r}_1 < 0$ for any value $k(\delta) < \pi/2$. Simulation has shown that larger values of k can indeed drive the system to be unstable. It is noticed, however, that for values of k near $\pi/2$, $\dot{r}_1$ approaches 0 as δ approaches 0 or π. Because trajectories that asymptotically spiral toward the target are undesirable, this condition will be further investigated.

The equation of motion for the angle θ_i is given by the following:

$$\dot{\theta}_i = (v_i/r_i)\sin(\theta_i - \psi_i) \tag{24}$$

The undesirable condition of spiraling trajectories would give a bearing angle that is continually changing. Equation (24) shows, however, that the bearing angle is constant for $\psi_i = \theta_i$. From Eq. (20), this condition is satisfied when $\delta = \pi/2$. The equation of motion for δ can be used to show that $\delta = \pi/2$ is a globally asymptotically stable equilibrium point.

Substituting the guidance law gives the following expression for $\dot{\delta}$:

$$\dot{\delta} = (v_1/r_1)\sin(-k(\delta)\sin(\delta - \pi/2)) - (v_2/r_2)\sin(k(\delta)\sin(\delta - \pi/2)) \tag{25}$$

The Lyapunov function $V = (\delta - \pi/2)^2$ is chosen. It is seen that $\dot{V}$ equals 0 at $\delta = \pi/2$ and $\dot{V} < 0$ for all other values of δ. Therefore, the trajectories generated by the feedback guidance will asymptotically converge to configurations with $\delta = \pi/2$ and constant bearing angles.

The performance of the feedback guidance will now be evaluated by applying Eq. (20) to problems 1 and 2. The feedback performance could be tested using a rigorous search for the optimal form of k, but here a form for k was selected through judicious tuning. For problem 1, a form of $k(\delta) = 1.21|\sin(\delta - \pi/2)|$ was chosen. This nonlinear gain gives greater emphasis on the perspective maneuvering when δ is near 0 or π and reduced emphasis as δ approaches $\pi/2$. This gain satisfies the stability condition because $k(\delta) < \pi/2$ for all values of δ. The resulting trajectories are shown in Fig. 6a. The resulting cost is $J = 1.594 \times 10^4$ s · ft^2 and the final time is $t_F = 8.051$ s. Although suboptimal, the cost here is within 0.05% of the cost found using the indirect method.

Applying field-of-view constraints to the feedback-guidance law is accomplished in a straightforward manner by placing bounds on the second term of Eq. (20). Note that such bounds do not invalidate the interception guarantee already demonstrated, because they do not

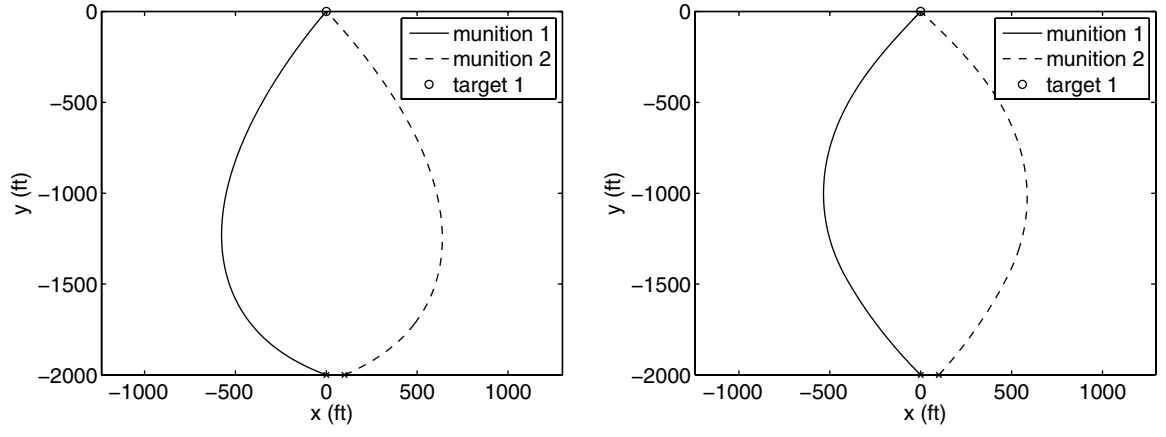

Fig. 6 Feedback-guidance trajectories: a) problem 1, and b) problem 2.

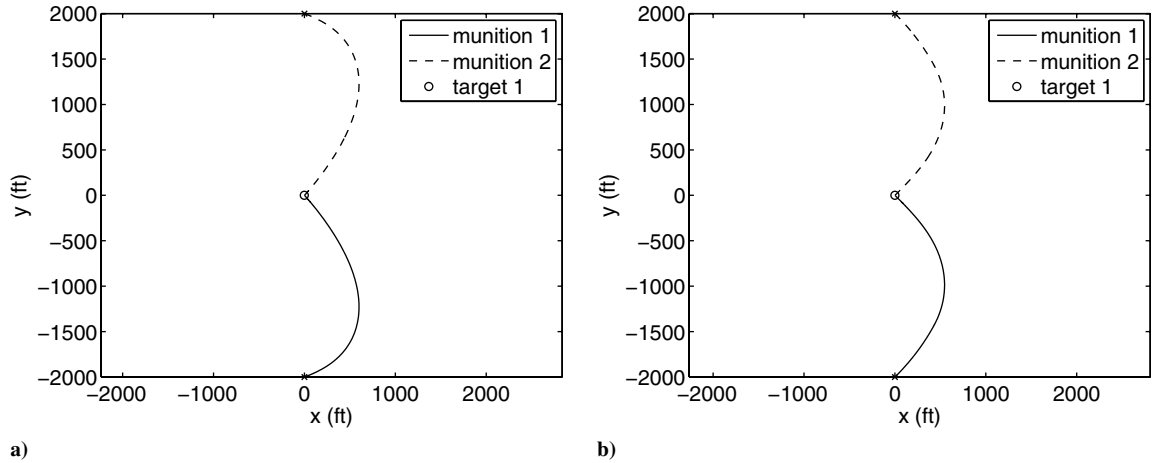

Fig. 7 Feedback-guidance trajectories: a) problem 3, and b) problem 4.

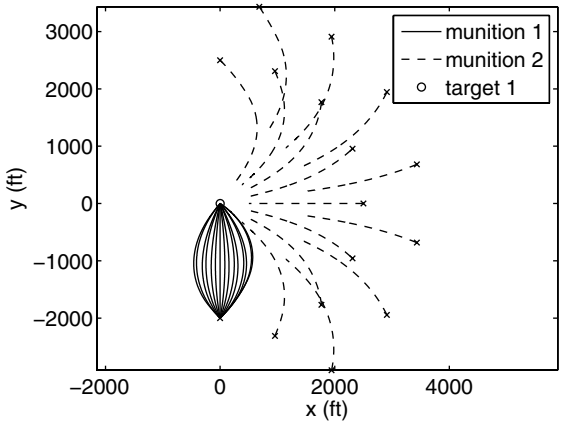

Fig. 8 Feedback-guidance trajectories for a selection of initial conditions.

change the sign of Eq. (23). For the solution of problem 2, the choice of $k = 0.95 \neq k(\delta)$ generates the trajectories shown in Fig. 6b. The associated cost is $J = 1.693 \times 10^4$ s $\cdot$ ft^2 and the final time is $t_F = 7.757$ s. This cost is within 1.1% of the cost found using the direct-shooting method.

Problems 3 and 4 can also be investigated using the feedback guidance with the same gain settings as problems 1 and 2, respectively. The resulting trajectories are shown in Fig. 7. For problem 3, the cost is $J = 1.894 \times 10^4$ s $\cdot$ ft^2 and the final time is $t_F = 8.151$ s, which is within 0.07% of the cost found using the indirect method. For problem 4, the cost is $J = 2.017 \times 10^4$ s $\cdot$ ft^2 and the final time is $t_F = 7.797$ s, which is within 1.2% of the cost found using the direct-shooting method.

These results show that the feedback-guidance law can be tuned to obtain a performance very close to the best known solution for some particular problems. A main benefit of the feedback law is that it can be used to quickly generate trajectories for various initial conditions. Implementation only requires the evaluation of Eq. (20) at each time instant. Good performance can be achieved for a large variety of initial conditions with a single gain value. Figure 8 demonstrates trajectories generated by feedback guidance with $k = 0.95$ and the field-of-view constraints enforced for a selection of different initial conditions.

V. Estimation Performance

The impact of the SLAP trajectories on the target-location estimation can now be evaluated. Although the trajectories were designed using a cost function based on the variances from a continuous WLSE algorithm, the estimation performance will be evaluated using a recursive weighted least-squares estimation (RWLSE) algorithm with discrete measurement updates. First, the algorithm will be operated for a single munition following a trajectory from the initial condition straight to the target location (STT trajectory). Second, the estimation is performed for two munitions both following STT trajectories. Finally, the algorithm is implemented using two munitions following the field-of-view constrained feedback-guidance trajectories presented in Sec. IV. In each case, noisy measurements were simulated using the measurement model in Eq. (4).

The munition sensors were assumed to collect measurements of the target location at a rate of 10 Hz. The RWLSE algorithm operated as follows to determine the estimate and the uncertainty at the kth time step [23,24]. The current estimate is computed as follows:

$$\mathbf{K}_k = \mathbf{P}_{k-1}\mathbf{H}^{\mathsf{T}}(\mathbf{H}\mathbf{P}_{k-1}\mathbf{H}^{\mathsf{T}} + \mathbf{R})^{-1} \tag{26}$$

$$\hat{\mathbf{x}}_k^{(T)} = \hat{\mathbf{x}}_{k-1}^{(T)} + \mathbf{K}_k(\tilde{\mathbf{z}}_k - \mathbf{H}\hat{\mathbf{x}}_{k-1}^{(T)}) \tag{27}$$

The current covariance matrix is computed as shown:

$$\mathbf{P}_k = \begin{bmatrix} \sigma_{x,k}^2 & \sigma_{xy,k} \\ \sigma_{xy,k} & \sigma_{y,k}^2 \end{bmatrix} = (\mathbf{P}_{k-1}^{-1} + \mathbf{H}_k^{\mathsf{T}}\mathbf{R}_k^{-1}\mathbf{H}_k)^{-1} \tag{28}$$

To compare the estimation performance along the different trajectories, the area of the 1σ uncertainty ellipsoid in the target-location estimate can be used as a metric. At the kth time step, this is given by the product of π with the square root of the product of the eigenvalues of $\mathbf{P}_k$. In particular, the ellipsoid size at $(t_F - 2)$ s will be highlighted. Although t_F is different for each trajectory, at this point in time munition 1 is roughly 600 ft from the target.

Using the initial condition of $x_1(0) = 0$ ft and $y_1(0) = -2000$ ft, the STT trajectory has a flight time given by $t_F = 6.67$ s. Using a single munition on an STT trajectory, at $(t_F - 2)$ s the 1σ uncertainty ellipse has an area of 81.5 ft^2, as shown in Table 2. For $x_2(0) = 100$ ft and $y_2(0) = -2000$ ft, adding measurements from munition 2 on an STT trajectory reduces the uncertainty to 39.7 ft^2. When the two munitions follow the SLAP trajectories shown in Fig. 6b, however, the area is reduced to 8.0 ft^2.

The error histories for a sample simulation with noisy measurements and 3σ error bounds ($\pm 3\sigma_{x,k}$ and $\pm 3\sigma_{y,k}$) generated by the RWLSE algorithm are shown in Fig. 9. Figure 9a shows the

Table 2 Uncertainty ellipsoid areas in ft^2 at $(t_F - 2)$ s for sample problems

Method	Problem 2	Problem 4
STT: single munition	81.5	81.5
STT: two munitions	39.7	40.8
SLAP: two munitions	8.0	8.3

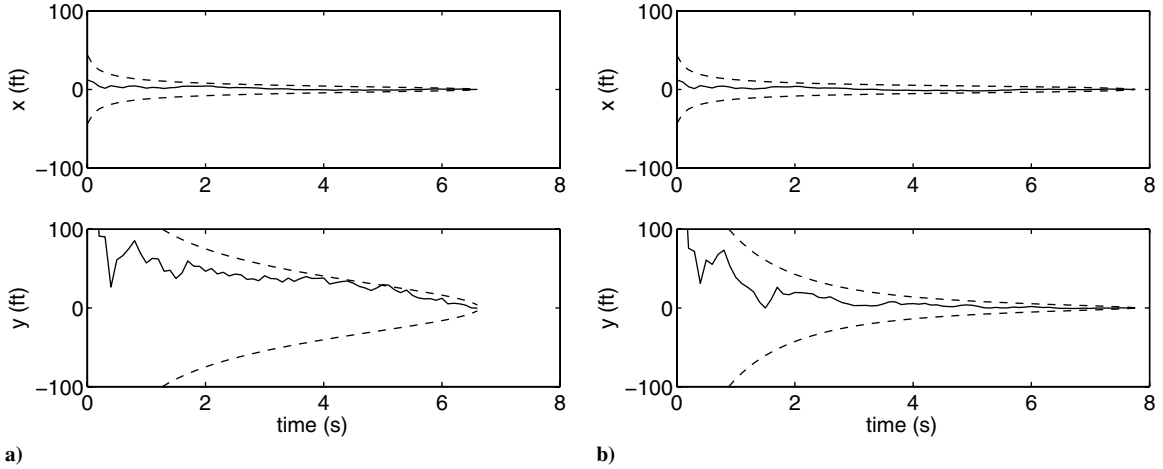

Fig. 9 Estimation errors with $x_2(0) = 100$ ft and $y_2(0) = -2000$ ft: a) STT, and b) SLAP trajectories.

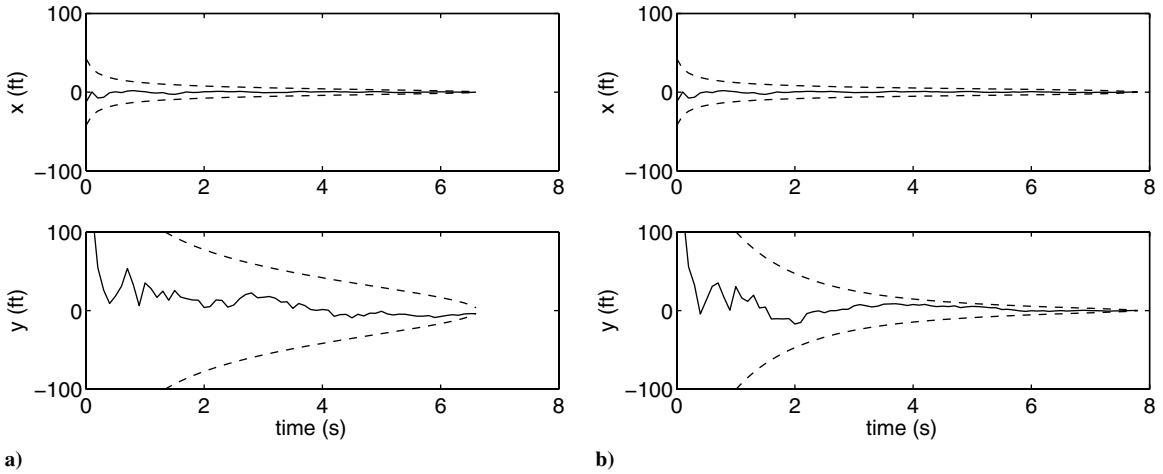

Fig. 10 Estimation errors with $x_2(0) = 0$ ft and $y_2(0) = 2000$ ft: a) STT, and b) SLAP trajectories.

errors in the x and y estimates of the target location using the STT trajectories. Figure 9b show the errors using the feedback-guidance trajectories. Clearly, both trajectories give a similarly good performance in estimating the x component of the target location, but the SLAP trajectories provide much better estimation of the y component.

Moving munition 2 to the initial condition of $x_2(0) = 0$ ft and $y_2(0) = 2000$ ft obviously does not change the results when only the measurements from munition 1 are considered. For the cases with two munitions, however, the uncertainty areas at $(t_F - 2)$ s are 40.8 ft^2 for the STT trajectories and 8.3 ft^2 for the SLAP trajectories. For these initial conditions, the error histories for a sample simulation with noisy measurements and 3σ error bounds generated by the RWLSE algorithm are shown in Fig. 10.

These results give an indication of the impact of trajectory design on estimation performance. Significantly, for either initial condition, adding a second munition to help in the target-location estimation without paying attention to trajectory design improves performance to approximately half of the uncertainty achieved with a single munition. Careful use of the SLAP trajectories, however, further reduces the uncertainty to less than one-quarter of what is achieved using the STT trajectories. The SLAP trajectories benefit both from being delayed, which allows collection of more measurements, and from their paths, which improve the quality of the measurements.

VI. Conclusions

The results in Sec. V demonstrate the impact that careful trajectory design can have on target-location estimation. Adding a second munition when following straight-to-target trajectories does significantly improve estimation performance. The use of the simultaneous-localization-and-planning trajectories, however, reveals further improvement. Furthermore, the complexity and cost of the second munition and communication between the two has already been accepted in taking the first step. The second step of following the simultaneous-localization-and-planning trajectories only requires careful trajectory design.

The development of a feedback-guidance approach brings the concept of cooperative attack closer to realistic implementation. The suboptimal feedback only requires evaluation of the guidance laws at each time step without the numerical search for solutions required by indirect and direct solution methods to the optimal control problem. Additionally, the demonstrations of global stability and excellent performance indicate strong potential for the feedback-guidance approach.

Improvements in estimation performance such as those demonstrated here could have a significant impact on munition design and cost. More accurate target-location estimation could allow for more accurate strike capability or the ability to attack targets that are difficult to detect. It is anticipated that the reduction in uncertainty early in the trajectory could be critical for the precision strike of these difficult targets; however, further work is needed to demonstrate the impact of these estimation enhancements on guidance and control performance. Combined, these effects could enable the use of smaller, cheaper munitions against targets in cluttered environments while limiting collateral damage.

References

[1] Chandler, P. R., Pachter, M., Nygard, K. E., and Swaroop, D., "Cooperative Control for Target Classification," *Cooperative Control and Optimization*, edited by R. Murphey, and P. M. Pardalos, Kluwer, Netherlands, 2002, pp. 1–19.

[2] Jeffcoat, D. E., "Coupled Detection Rates: An Introduction," *Theory and Algorithms for Cooperative Systems*, edited by D. Grundel, R. Murphey, and P. M. Pardalos, World Scientific, Hackensack, NJ, 2004, pp. 157–167.
[3] Frew, E., and Lawrence, D., "Cooperative Stand-Off Tracking of Moving Targets by a Team of Autonomous Aircraft," AIAA Paper 2005-6363, Aug. 2005.
[4] Speyer, J. L., Hull, D. G., Tseng, C. Y., and Larson, S. W., "Estimation Enhancement by Trajectory Modulation for Homing Missiles," *Journal of Guidance, Control, and Dynamics*, Vol. 7, No. 2, 1984, pp. 167–174. doi:10.2514/3.8563
[5] Hull, D. G., Speyer, J. L., and Tseng, C. Y., "Maximum-Information Guidance for Homing Missiles," *Journal of Guidance, Control, and Dynamics*, Vol. 8, No. 4, 1985, pp. 494–497. doi:10.2514/3.20010
[6] Fawcett, J. A., "Effect of Course Maneuvers on Bearings-Only Range Estimation," *IEEE Transactions on Acoustics, Speech, and Signal Processing*, Vol. 36, No. 8, 1988, pp. 1193–1199. doi:10.1109/29.1648
[7] Hammel, S. E., Liu, P. T., Hilliard, E. J., and Gong, K. F., "Optimal Observer Motion for Localization with Bearing Measurements," *Computers & Mathematics with Applications*, Vol. 18, Nos. 1–3, 1989, pp. 171–180. doi:10.1016/0898-1221(89)90134-X
[8] Logothetis, A., Isaksson, A., and Evans, R. J., "Comparison of Suboptimal Strategies for Optimal Own-Ship Maneuvers in Bearings-Only Tracking," *1998 American Control Conference*, IEEE Publications, Piscataway, NJ, June 1998, pp. 3334–3338. doi:10.1109/ACC.1998.703192
[9] Passerieux, J.-M., and VanCappel, D., "Optimal Observer Maneuver for Bearings-Only Tracking," *IEEE Transactions on Aerospace and Electronic Systems*, Vol. 34, No. 3, 1998, pp. 777–788. doi:10.1109/7.705885
[10] Oshman, Y., and Davidson, P., "Optimization of Observer Trajectories for Bearings Only Target Localization," *IEEE Transactions on Aerospace and Electronic Systems*, Vol. 35, No. 3, 1999, pp. 892–902. doi:10.1109/7.784059
[11] Frew, E. W., and Rock, S. M., "Trajectory Generation for Constant Velocity Target Motion Estimation Using Monocular Vision," *IEEE International Conference on Robotics & Automation*, IEEE Publications, Piscataway, NJ, Sept. 2003, pp. 3479–3484.
[12] Watanabe, Y., Johnson, E. N., and Calise, A. J., "Vision-Based Guidance Design from Sensor Trajectory Optimization," AIAA Paper 2006-6607, Aug. 2006.
[13] Grocholsky, B., "Information-Theoretic Control of Multiple Sensor Platforms," Ph.D. Thesis, Univ. of Sydney, Sydney, Australia, 2002
[14] Ousingsawat, J., and Campbell, M. E., "Optimal Cooperative Reconnaissance Using Multiple Vehicles," *Journal of Guidance, Control, and Dynamics*, Vol. 30, No. 1, 2007, pp. 122–132. doi:10.2514/1.19147
[15] Dohner, J. L., Eisler, G. R., Driessen, B. J., and Hurtado, J., "Cooperative Control of Vehicle Swarms for Acoustic Target Localization by Energy Flows," *Journal of Dynamic Systems, Measurement, and Control*, Vol. 126, No. 4, Dec. 2004, pp. 891–895. doi:10.1115/1.1852463
[16] Passino, K., Polycarpou, M., Jacques, D., Pachter, M., Liu, Y., Yang, Y., Flint, M., and Baum, M., "Cooperative Control for Autonomous Air Vehicles," *Cooperative Control and Optimization*, edited by R. Murphey, and P. M. Pardalos, Kluwer, Netherlands, 2002, pp. 233–271.
[17] Pachter, M., and Hebert, J., "Cooperative Aircraft Control for Minimum Radar Exposure," *Cooperative Control and Optimization*, edited by R. Murphey, and P. M. Pardalos, Kluwer, Netherlands, 2002, pp. 199–211.
[18] Zabarankin, M., Uryasev, S., and Pardalos, P., "Optimal Risk Path Algorithms," *Cooperative Control and Optimization*, edited by R. Murphey, and P. M. Pardalos, Kluwer, Netherlands, 2002, pp. 273–303.
[19] Murphey, R., Uryasev, S., and Zabarankin, M., "Optimal Path Planning in a Threat Environment," *Recent Developments in Cooperative Control and Optimization*, edited by S. Butenko, R. Murphey, and P. Pardalos, Kluwer, Netherlands, 2004, pp. 349–406.
[20] Kabamba, P. T., Meerkov, S. M., and Zeitz, F. H., III, "Optimal Path Planning for Unmanned Combat Aerial Vehicles to Defeat Radar Tracking," *Journal of Guidance, Control, and Dynamics*, Vol. 29, No. 2, 2006, pp. 279–288. doi:10.2514/1.14303
[21] Pachter, M., Chandler, P. R., Purvis, K. B., Waun, S. D., and Larson, R. A., "Multiple Radar Phantom Tracks From Cooperating Vehicles Using Range-Delay Deception," *Theory and Algorithms for Cooperative Systems*, edited by D. Grundel, R. Murphey, and P. M. Pardalos, World Scientific, Singapore, 2004, pp. 367–390.
[22] Purvis, K. B., Chandler, P. R., and Pachter, M., "Feasible Flight Paths for Cooperative Generation of a Phantom Radar Track," *Journal of Guidance, Control, and Dynamics*, Vol. 29, No. 3, 2006, pp. 653–661. doi:10.2514/1.15563
[23] Stengel, R. F., *Optimal Control and Estimation*, Dover, New York, 1986.
[24] Crassidis, J. L. and Junkins, J. L., *Optimal Estimation of Dynamic Systems*, Chapman & Hall/CRC Press, Boca Raton, FL, 2004.
[25] Boyd, S., and Vandenberghe, L., *Convex Optimization*, Cambridge Univ. Press, Cambridge, England, U.K., 2004, Chap. 3.
[26] Sinclair, A. J., Prazenica, R. J., and Jeffcoat, D. E., "Simultaneous Localization and Planning for Cooperative Air Munitions," *Advances in Cooperative Control and Optimization*, edited by R. M. Michael, J. Hirsch, P. M. Pardalos, and D. Grundel, Vol. 369, Lecture Notes in Control and Information Sciences, Springer–Verlag, New York, 2007, pp. 81–94.